On the Quest of Small Molecules that Can Mimic Psalmotoxin-1, a Powerful Peptidic Modulator of the Acid Sensing Channel ASIC1a

Francesco Pietra (chiendarret@gmail.com)
Accademia Lucchese https://orcid.org/0000-0003-3215-5376

Research Article

Keywords: ion channels, spider toxins, PcTx1, QM-MM, MEP

Posted Date: June 15th, 2021

DOI: https://doi.org/10.21203/rs.3.rs-467127/v1

Abstract

Acid-sensing ion channels (ASICs) are thought to play a key role in a number of pathologies, from neuronal injury to pain sensation, while no drug has yet been approved as their modulator. This work was devised to asses roughly, yet from first principles, the relative energies of binding in the most important acidic pocket of cASIC1a, thereby paving the way to find small molecules that can mimic Pctx1, the most powerful peptidic modulator of cASIC1a. To this end, MD simulations for the overall conformation, and QM-MM simulations specifically for the location of hydrogen atoms, allowed disentangling the relative weight of the various non-bonded interactions between PcTx1 and cASIC1a. Main weight could be attributed to deeply buried salt bridges formed by the guanidinium end chains of residues Arg26 and Arg27 on PcTx1 and carboxylate end chain of distant residues Asp and Glu on cASIC1a. Rewardingly, in a preliminary attempt at exploiting these observations toward a small-molecule modulator, a Arg26-Arg27 stretch, excised from the PcTx1-cASIC1a complex and slightly simplified, on automated rigid docking on ligand-free receptor was observed to form most of the above salt bridges.

1. Introduction

Acid-sensing ion channels (ASICs) are low-pH activated Na^+-permeable ion channels encoded, as far as it is presently known, by four genes to give homo- and hetero-trimeric ASIC1a, ASIC1b, ASIC2a, ASIC3, and ASIC4 [1]. They are widely expressed in central and peripheral nervous systems and are believed to be involved with many pathologies, like neuronal injury, pain sensation and seizure, while affecting synaptic function and plasticity [2]. Therefore, ASICs represent foreseeable drug targets, particularly as far as pain and ischemic stroke are concerned, although this goal has remained underdeveloped for a number of reasons. First of all, powerful exogenous modulators of ASIC channels had only been found with peptides of forty or more residues, which are prone to rapid degradation in blood plasma [3]. Second, the task was faced with a penury of structural data at atomic resolution, limited to the cASIC1a channel, achieved through X-ray diffraction at ca 3.0 Å resolution while leaving the architecture of the cytoplasmic terminal domains largely elusive [4]. Third, such structural limitations persisted for complexes with modulators, such as that of cASIC1a with the Tarantula peptide Psalmotoxin-1 (PcTx1) [5][6]. It is also to be noticed that the ASIC3 channel is particularly neglected, despite evidence that, by exhibiting high expression in sensory neurones while upon activation not being fully inactivated, it is a particularly interesting analgesic target [7].

These obstacles toward efficient small-molecule modulators of ASIC channels are now beginning to be removed. From one side, like in all areas of structural biology, cryo-electron microscopy is moving forward also with ASICs, having recently allowied to tackle for the first time human ASICs. This led to unravel the structure of hASIC1a and its complex with the black mamba peptide mambalgin-1 at 3.56 and and 3.90 Å resolution [8]. This fast moving technique has also recently allowed to unravel the whole apo structure of the cASIC1a channel, both in the pH = 7.0 desensitized and the pH = 8.0 resting conformations, at resolutions of ~ 2.8 and 3.7 Å, clarifying details of the way the channel works [9]. Importantly, when present work was nearly completed, two powerful small-molecule modulators of cASIC1a and rASIC1a have been presented, which, however, involve an acidic pocket different from those known for the long peptides [10].

What is still completely lacking is a quantitative evaluation of the relative importance of the various non-bonded interactions between ASIC channels and their modulators, which could help modeling the long sought small molecules that can powerfully modulate the ASICs. This work was conceived to pave the way toward such small molecules by investigating *in silico* the complex between the ion channel cASIC1a and the spider peptidic toxin PcTx1. The choice of PcTx1 was suggested by it being the most powerful modulator of ASIC1a at the most important acidic pocket, while other acidic pockets proved to be of lesser importance [11][12]. On the other hand, at the onset of this study, structural data at atomic resolution were only available for the PcTx1-cASIC1a complex [5].

As only protein residues are involved in the PcTx1-cASIC1a complex, for classical molecular dynamics (MD) simulations recourse was taken here to a long established fixed-charge classical force field rather than more elaborated force fields that

are at an earlier stage of development. The same approach was taken for quantum mechanics-molecular mechanics (QM-MM) simulations, where the MD force field was coupled to a widely established QM code, as detailed in the following.

2. Results And Discussion

This work has taken the challenge of evaluating in an aqueous medium the relative energies of the non-bonded interactions between the cASIC1a channel and its powerful modulator, the Tarantula peptide toxin Psalmotoxin-1 (PcTx1) [5][6]. Doing that by MD in aqueous solution allows viewing the cASIC1a-PcTx1 complex in a dynamic status, a task that the crystal data [5][6] cannot grant. In addition, to avoid any deterministic bias possibly introduced by the classical MD force field, the geometry at the interaction loci was re-assessed from first principles through QM-MM simulations with Density Functional Theory (DFT) with functional that are most suited for structural analysis, aided by account for dispersion, as detailed in the following.

To the above purpose, two models were built, as detailed in the Experimental Section, from the crystal structure at low pH (5.5) and high pH (7.25) of the cASIC1a-PcTx1 complex [5], i.e., primarily relying on the ligand-receptor interactions that resulted from the crystal study [5]. All missing atoms on both PcTx1 and the channel extracellular part were implemented while nearly all transmembrane domains were removed to alleviate the computational burden. While each subunit of the homotrimer hosts a PcTx1 molecule, only one was dealt with in this work. This is shown in Fig. 1 for the low pH complex, where PcTx1 (labeled as chain M, in red) inserts between chain A (yellow) and C (blue) of the homotrimer, digging deeply into the acidic pocket. To give a rough perspective of the spot, key residues are highlighted in Fig. 1 on both the ligand and the receptor. Residue R26 of PcTx1 gets close to D350 on chain C, while the adjacent R27 (not shown) does so with E220 on chain A of the receptor. Actually, it is only when the side chains are displayed in full for these residues that distances can be fully appreciated, as shown in the following. Highlighting residue F30 only serves to give a perception of the ligand sequence.

Each model was subjected to MD without any restraint on any atom, except for applying harmonic forces to where the transmembrane domains had been cut. For the QM-MM simulations all interacting residues between PcTx1 and cASIC1a were included, as resulting from the X-ray diffraction study of the crystal [5]. Water molecules that, from MD, turned out to be interacting with the selected peptidic residues were also added. In order to avoid duplication of statements, all interacting residues, as included in the QM-MM simulations, are indicated in the following Table 1 for the low pH and Table 2 for the high pH systems. Each complex was divided into the same four zones that were sketched in the original X-ray diffraction study for the low pH complex [5]. Each zone pivots on one or two PcTx1 residues, R26, R27, R28, and W7-W24, which interact with the closest residues on chains A and C of the homotrimer. Each zone was subjected separately to MD, followed by QM-MM simulations. The reason for the latter was to assess from first principles the hydrogen bonds which are not treated in depth by the fixed-charge force field of classical MD.

The results for the low pH complex are compiled in Table 1. The first column lists the PcTx1 residues that interact with those of cASIC1a in the second column, specifying, in the order, chain name, residue name and number, and atom name. Columns 3 to 6 tabulate the interatomic distances corresponding to the first two columns, the third column listing crystal data [5]. In the fourth column data are reported for the pre-MD, minimized model in aqueous solution with restraints only applied to where the transmembrane domains had been cut. The fifth column reports data for averaged distances from MD simulations. The sixth column lists averaged distances from QMMM simulations. The seventh column tabulates the interaction non-bond energies between the residues in columns 1-2, highlighting in boldface key values. Finally, the last column shows the HOMO-LUMO energy gap for each group of interactions. A similar compilation of data can be seen in Table 2 for the high pH complex.

Table 1. Geometry and non-bonded interaction energy for the PcTx1-cASIC1a complex under low pH (5.5) conditions

PcTx1 Chain/Residue/Atom	CASIC1a Chain/Residue/Atom	Interatomic distances (Å), choosing the couple of atoms at shortest distance, which is indicated when they differ with respect to the crystal structure				Inter-residues non-bond energy from QMMM	HOMO-LUMO gap kcal mol^{-1}
		Crystal[a)]	Minimized	MD[b)]	QMMM[b)]	kcal mol^{-1}	
M/W7/CG	C/F351/CG	7.7	7.6	8.0	7.9	+1.1 ±2.9	124.5
M/W24/CG	C/F351/CG	6.7	6.9	7.4	7.2	-1.5 ±1.0	
M/R26/NH2	M/S29/OG	3.0	3.2	3.1	6.3	-0.3 ±2.0	131.4
M/R26/NH2	M/F30/O	2.9	3.7	3.4	4.0	**-15.6 ±1.5**[c)]	
M/R26/NH1	C/D350/OD2	3.3	2.7	4.2	2.7	**-40.4 ±3.9**[d)]	
M/R26/NH2	C/D238/OD2	4.0	2.6 (NH1 OD1)		3.4	**-29.1 ±3.0**[d)]	
C/R191/NH2	C/D350/OD1	3.3	2.7 (NH1)	2.6 (NH1)	2.7 (NH1)	**-54.8 ±4.3**[d)]	
C/R191/NH1	C/D238/OD1	2.9 (NH2)	3.5 (NH2)	6.8 (NH2 OD2)	6.0 (NH2 OD2)	No stabilization	
M/R26/NH2	H_2O/9058				3.5	+3.5 ±1.5	
M/R27/NH2	A/T215/O	3.6	2.8	5.6 (NH2)	5.3 (NH2)	+0.16 ±1.2	138.4
M/R27/NH2	A/G216/O	3.3	4.9	8.5	7.8 (NH2)	-0.86 ±0.35	
M/R27/NH2	A/G218/O	3.1	4.6	7.7	7.4 (NH2)	-0.14 ±0.25	
M/R27/NH1	A/E220/OE2	3.4	2.7 (OE1)	3.1 (NH2 OE1)	2.8 (NH2 OE1)	**-46.3 ±3.2**[d)]	
M/R27/NH1	A/D408/OD2	4.2	2.6 (NH2)	2.7 (NH2 OD1)	3.0 (NH2 OD1)	**-53.1 ±6.1**[d)]	
M/R27/NH2	H_2O/2258				4.3	+1.8 ±1.1	
A/219/N	H_2O/2258				3.8		
M/R28/NH1	C/D238/O	2.8	2.8	2.8	2.9		106.1
M/R28/O	C/D238/N	3.9	6.8	4.6	4.6	**-14.6 ±2.4**[c)]	

M/R28/NH2	C/T240/O	2.7	2.7	4.3 (NH1)	5.0 (NH1)	**-5.1 ±0.7**[c]
M/R28	H_2O/5909				7.7 (NH1)	-0.24 ±0.45

[a] From pdb file 4FZ0 [5]

[b]Averaged positions.

[c]H-bond.

[d]H-bond and salt-bridge.

In parallel, molecular electronic potential maps (MEP) for each group of interactions, as in Table 1 and 2, are visualized in the next four illustrations. Comparisons are aided by placing side to side, for each group of interacting residues, MEPs for the low and the high pH systems. As these MEPs were built directly from the QM code, they require more attention than any *a posteriori* illustration from presentation graphics software. The extra attention is more than repaid by a direct view on what was going on with the computation from first principles. What also helps, are chain, residue and atom labels set in a 3D perspective, in the same color as the corresponding atoms. High negative and positive potentials are highlighted in blue and red, respectively, with intermediate colors for intermediate potentials. Finally, by making the MEPs translucent, the underlying molecular skeleton can be seen, where the interacting atoms, corresponding to Table 1 and 2, are highlighted at 25% of the vdW size, in blue for nitrogen and red for oxygen.

All that said, we are now in a position to analyze the results of this study. First about the very high values of the HOMO-LUMO energy gap, which speaks for high stability of the complex in solution, accompanied by some conformational changes, as discussed in the following. It also comes to the eyes the extremely small stabilizing non-bond energy for the aromatic ‘embrace’ between W7 and W24 of PcTx1 and F351 of cASIC1a for both the low (Table 1) and the high pH complex (Table 2). Concerned is a residue, F351, that lies in a small region important for pH-dependent gating and PcTx1 modulation of ASIC1a [13].

What confidence is deserved by the non-bond energies in Table 1 and 2, as disentangled with the NAMDenergy plugin? The short answer is that the NAMDenergy plugin gives what the force field used, CHARMM36, can give. This was applied to the ensemble in a periodic box under Particle Mesh Ewald (PME) conditions, thus taking also full electrostatic interactions into account. In addition, it is important noticing that the NAMDenergy plugin was applied to structures geometrically tempered with QM-MM simulations, i.e., by using first principles, which, as said above, is particularly important for hydrogen bonds, which are not treated in depth by the fixed-charge CHARMM36 force field. With the aromatic ‘embrace’, visualized by the MEP maps of Fig. 2, the attractive forces are limited to dipole-dipole, dipole-induced dipole, and London (dispersion) interactions, treated in terms of the Lennard-Jones potential. No strong electrostatic forces come into play.

Table 2. Geometry and non-bonded interaction energy for the PcTx1-cASIC1a complex under high pH (7.25) conditions

PcTx1 Chain/Residue/Atom	CASIC1a Chain/Residue/Atom	Interatomic distances (Å), choosing the cuple of atoms at shortest distance, which is indicated when they differ with resoect to the crystal structure				Inter-residue non bond energy	HOMO-LUMO gap kcal mol^{-1}
		Crystal[a)]	Minimized	MD[b)]	QMMM[b)]	kcal/mol	
M/W7/CG	C/F351/CG	8.5	8.4	8.4	8.1	-1.8 ±0.7	106.1
M/W24/CG	C/F351/CG	7.4	8.3	6.5	6.3	+9.3 ±22.0	
M/R26/NH2	M/S29/OG	3.7	3.3	3.5	3.5	+1.6 ±2.5	133.8
M/R26/NH2	M/F30/O	3.1	5.0	6.0	5.6	**-8.9 ±1.0**[c)]	
M/R26/NH1	C/D350/OD2	3.0	2.7	2.8	2.9	**-34.2 ±3.2**[d)]	
M/R26/NH1	C/D238/OD1	3.7	2.9	4.7 (OD2)	4.3	**-7.7 ±1.6**[d)]	
C/R191/NH2	C/D238/OD1	3.3	2.6	2.6 (NH1 OD2)	3.0 (NH1 OD2)	**-44.6 ±3.2**[e)]	
M/R26/NH2	H_2O/721				3.2	-1.7 ±1.9	
M/R27/NH1	A/T215/O	3.6	2.9	4.0	4.3	**-4.2 ±0.6**[c)]	117.8
M/R27/NH2	A/G216/O	3.0	3.0	3.5	3.7	**-7.8 ±1.2**[c)]	
M/R27/NH2	A/G218/O	2.8	4.2	2.8	2.8	**-18.6 ±1.5**[c)]	
M/R27/NH1	A/E220/OE2	3.4	2.7	3.4	2.8	**-34.0 ±1.1**[d)]	
M/R27/NE	H_2O/1718				3.3	+4.9 ±1.6	
M/R28/NH2	C/D238/O	5.4	4.9	5.7 (NH1)	6.7 (NH1)	+8.0 ±0.8	76.1
M/R28/O	C/D238/N	3.9	3.9 checked	3.9	3.3		
M/R28/NH2	C/T240/O	4.6	2.7	3.3 (NH1)	4.1 (NH1)	**-3.2 ±1.1**[c)]	

M/R28/N	H_2O/3514			2.9	**-5.4 ±2.4**[c)]

a) From pdb file 4FZ1 [5].

b) Averaged positions avpos.

c)H-bond.

d)H-bond and salt-bridge.

e)Salt-bridge.

Quite different are all other groups of interactions, pivoting on R26, R27 and R28 of PcTx1. With these, high values of non-bond energy are highlighted in boldface in the sixth column of Table 1 and 2. With the R26 group for the low pH complex (Table 1), two highly stabilizing interactions occur between R26 on PcTx1 and the protein residues D350 and D238, and a smaller one, inside PcTx1, between R26 and F30.[1] The latter is mainly accounted for by only a hydrogen bond, while with the other interactions a complete salt bridge, generated by the interaction of a carboxylate with a guanidinium group, comes into play. This is visualized by the MEP maps of Fig. 3, left. Notably, there is no stabilizing interaction between residues R191 and D238, contrary to expectations from the crystal structure, (third column, same row) [5]. Under MD the side chains for these two residues were moved away from one another, the distance between R191/NH1 and D238/OD1 becoming as large as 6.8 Å. This remained nearly unaltered under QM-MM simulations, speaking for lack of stabilization. That is not the case of the high pH complex, where a salt bridge is retained between R191 and D238 (Table 2 and Fig. 3, right). To this concern, it is to be noticed that a salt bridge without any hydrogen bond was established by QM-MM simulations between R191 and D238. Despite the lack of any hydrogen bond, a quite high non-bond energy was calculated for such interaction.[1] These observations indicate that PcTx1, in order to stick to the trimer, was mainly looking for interactions that generate a salt bridge.

With the group pivoting on residue R27 of PcTx1, a non-bonded interaction with E220 of chain A, generating a salt bridge, occurs with both the low and the high pH complexes. This is reported in Table 1 and 2 and visualized in Fig. 4. Otherwise, the two complexes differ markedly as to non-bonded interactions. The low pH complex is strongly stabilized by non-bonded interactions between R27 of PcTx1 and D408 of the receptor, while no such interaction occurs with the high pH complex, replaced by a hydrogen bond with G218.

With the last group of interacting residues, the one pivoting on R28 of PcTx1, it is seen from Table 1 and 2, and illustrated in Fig. 5, that, once the highly stabilizing salt bridges are set in place with R26 and R27, R28 can only interact with the trimer via hydrogen bonds. This explains why low non-bond energies were calculated in this case, especially low for the high pH complex.

From all these observations it was devised here to model a ligand that could form salt bridges with the two most important couples of residues as from Table 1, i.e., D238 and D350 on chain C for R26, and the distant E220 and D408 on chain A for R27. In a first attempt, a R26-R27 stretch was excised from PcTx1 in the complex with cASIC1a for the low pH complex, as equilibrated with MD (Fig. 6, top). Unfilled valencies were satisfied by changing both CHO and NH to H, while imposing the rigid conformation of the crystal that fixes the two guanidinium ends at at distance of nearly 10 Å as required to interact with the widely separated carboxylates (Fig. 6, bottom). This modifiied-R26-R27 molecule was used for automated rigid-body docking on the complex freed from PcTx1. It was a pleasure observing that three of the expected salt bridges were formed, to D408 and E220 from one side and D238 from the other side (Fig. 7), mimicking the allosteric way of doing of PcTx1.[4] Admittedly, this is an artificial first approach to modeling a ligand that, by exploiting only a few points of binding to the receptor, docks into the most important acidic pocket of ASIC1a in the way that PcTx1 does. Nonetheless, this simple

approach shows that modeling an apprppriately rigid small molecule that, by avoiding any great entropy loss, imitates the mode of binding of PcTx1 to ASIC1a should be possible.

3. Conclusions

A quantitative analysis carried out in this work of the distribution of non-bonded forces acting within the PcTx1 acidic pocket of cASIC1a in aqueous solution has shown a strict cooperativity of forces, like in a spider web. Nonetheless, MD and QM-MM simulations revealed that the non-bonded interactions that contribute most to the stability of the complex are salt bridges formed between end-chain guanidinium functionalities of PcTx1 and end-chain carboxylates of cASIC1a.

Fulfilling the aim of furnishing indications as to model a small molecule that retains the ability of PcTx1 of allosterically modulating the receptor, the above results suggested to armor a small molecule of two guanidinium teeth that can grasp to carboxylate ends that are separated by as much as nearly 10 Å, in the acidic pocket. This was implemented by excising a R26-R27 stretch from PcTx1 and modifying it to saturate the unfilled valencies. Rewardingly, on automated rigid-body docking of this stabilized R26-R27 molecule on the ligand free complex, most of the expected salt bridges were formed, as it occurs with the PcTx1-cASIC1a complex.

Treating in silico protein systems is a very challenging undertaking, if not else because their structural stability is strikingly dependent from the in vivo environment [15]. However, this simple in silico approach allowed observing the dynamics in the acidic pocket and the forces involved, complementing the static view from X-ray diffraction. This should prove of heuristic value in designing an effective modulator of ASICs.

4. Experimental Section

Modeling: The receptor was modeled on the X-ray diffraction crystal structure of the complex between PcTx1 and cASIC1a at either low (5.5) or high pH (7.25), 2.8 and 3.0 Å resolution, Protein Data Bank, PDB code 4FZ0 and 4FZ1, respectively [5]. Both NAG (2-acetamido−2-deoxy-beta-d-glucopyranose) and GOL (propane−1,2,3-triol) residues were discarded and the following residues were eliminated from the intracellular domains, without capping: 50–71 and 427–454 of chain A, 45–70 and 425–450 of chain B, as well as 42–71 and 426–451 of chain C. All missing residues, or part thereof, were implemented with software MODELLER [16]. Titrable residues were dealt with on the H++ server [17] by using internal and external dielectric, 10 and 80, respectively, salinity 0.15 m and pH 5.5 or 7.25 for the low and high pH ensemble, not allowing for any side chain reorientation. Histidine protonation turned out to be as follows (residue name/residue number) for the low pH complex (chain/residue number). HSE: A/164/328, B/328, C/328; HSP: A/74/111/251, B//74/111/164/251, C/74/111/164/251, while for PcTx1 HSP 14 throughout. For the high pH complex, HSE: A/164, B/164, C/164; HSD: A/74/111/251/328, B/74/111/251/328, C/74/111/251/328, while for PcTx1 HSD 14 throughout. All water belonging to the extracellular part was retained. Generation of psf/pdb file, while adding all missing H-atoms and establishing all disulfide bonds, was carried out with AutoPSF included in software VMD v 1.9.3 [18], with force field CHARMM36 [19], and solvating in a periodic box with TIP3 water with 12 Å padding, while neutralizing and adding 0.15M NaCl. For the low pH complex, this resulted in a box of dimensions x = 123, y = 125, z = 115 Å for a total of 167716 atoms, 51019 residues, of which 49520 waters, while for the high pH complex, box dimensions x = 126, y = 117, z = 111 Å, for a total 153479 atoms, 46249 residues, of which 44776 waters.

Methods : Minimization of the above ensembles was carried out with software NAMD, v 2.13 [20] by first restraining all atoms except water and then only the residues where the transmembrane domains had been cut. Gradual heating to 310K was followed by constant number, volume and temperature (NVT) and then constant number, pressure and temperature (NPT) simulations with restraints like for minimization. The integrator timestep was kept as low as 1.0 fs to allow treating adequately vibrations involving H-atoms under Langevin stabilization with low damping and target 1.01325 bar, under PME and with 1-scaling. Rigid bonds were only used for water molecules. Constant RMS during NPT for the low pH ensemble

was reached with 18 ns trajectory and was continued to 30 ns. For the high pH ensemble shorter trajectories of 10 and 15 ns were sufficient. Averaged distances, as in Table 1 and 2, are from the avpos algorithm available with VMD software[18]. The QM-MM simulations were set up according to the same general methodology previously used with complexes between small molecules and ribosome [21], while subdividing the system into four zones for the interactions of PcTx1 key residues R26, R27, R28, and W7-W24 with the protein trimer, as delineated for the crystal structure [5]. The atoms included in the QM part were detailed above along the text and are specified in Tables 1 and 2. The method used here for electrostatic embedding, that is, electrostatic interactions between QM and MM atoms, was described in detail in the literature [22] and online documents [23]. In short, the partial charges of MM atoms surrounding all QM atoms are used here to approximate the electrostatic environment where QM atoms are found. QM-MM simulations were carried out with NAMD QM-MM software [22] based on NAMD software v. 2.13 [20\] and linked to ORCA software v. 4.2.1 [24]. Conditions for the MM part were temp 310 K, pressure 1.01325 bar, integrator timestep 1.0 fs, and cutoff = 12.0 Å. Main commands passed by NAMD to ORCA to implement DFT calculations were (I) use functional PBE0 with flags RIJCOSX, D3BJ for dispersion correction, and def2-SVP, and (ii) read molecular orbitals, so that the simulation could be restarted. On a single node, 34 cores for ORCA and one core for NAMD led to the fastest simulations. NAMD trajectories with QM-MM were 70, 3.5, 3.3, 4.5 ps for the ensembles pivoting on W7-W24, R26, R27, R28, respectively.

Docking. The model for automated docking was built from the R26-R27 residues excised from the averaged coordinates for all set of NPT equilibrations with the low pH complex and then modified by changing both O and NH into H as previously illustrated. Docking with rigid ligand and ligand-deprived low pH receptor was carried out with MGLtools v 1.5.6 [25] and AutodockVina v 1.1.2 [26] by selecting the central region of the receptor, by setting center and size of the grid, exhaustiveness 50, num_modes 20, and energy_range 5.

Data Analysis and Illustrations. The results were analyzed with VMD software [18] using the tools provided by NAMD QM-MM [23] and by ORCA [24] GNUplot [27] CHIMERA [28] and Jmol software [29]. Illustrations 2–5 were arranged with Jmol and 1, 6 and 7 with CHIMERA.

Declarations

Acknowledgments

The author gratefully acknowledges the CINECA consortium for the award cASIC1-HP10C8KQFV under the ISCRA initiative, which allowed generous access to high-performance computing resources.

Ethical approval: The author declares to have followed all indications in the section “Compliancve with Ethycal Standards” and not to be infringing any of them.

Funding: Funding to this work was granted by the CINECA consortium, award cASIC1-HP10C8KQFV under the ISCRA initiative, which only granted access to to high-performance computing resources.

Conflict of interest/Competing interest: The author has no conflict of interest and no competing interest to declare.

Availability of data and material: Supplementary material is included in the submission.

Code availability: not applicable as no new code was used in this work.

Authors’ contributions

This is a single author contribution. Everything was contributed by the single author, Francesco Pietra.

References

1. Bartoi T, Augustinowski K, Polleichtner G, Gründer S, Ulbrich MH (2014) **Acid-sensing ion channel (ASIC) 1a/2a heteromers have a flexible 2:1/1:2 stoichiometry**. *PNAS 111*: **8281–8286**
2. González-Inchauspe C, Urbano FJ, **Di** Guilmi MN, Uchitel OD (2017) **Acid-sensing ion channels activated by evoked released protons modulate synaptic transmission at the mouse calyx of Held synapse**. *J Neurosci 37*: **2589–2599**
3. Vullo S, Kellenberger S (2020) **A molecular view of the function and pharmacology of acid-sensing ion channels**. *Pharmacological Research 154*: **104166–104174**
4. Jasti J, Furukawa H, Gonzales EB, Gouaux E (2007) **Structure of acid-sensing ion channel 1 at 1.9A resolution and low pH**. *Nature 449*: **316–323**
5. Baconguis I, Gouaux E (2012) **Structural plasticity and dynamic selectivity of acid sensing ion channel–toxin complexes**. *Nature 7416*: **400–405**
6. Dawson RJ, Benz J, Stohler P, Tetaz T, Joseph C, Huber S, Schmid G, Hugin D, Pflimlin P, Trube G, Rudolph MG, Hennig M, Ruf A (2012) Structure of the Acid-sensing ion channel 1 in complex with the gating modifier Psalmotoxin 1. Nat Commun 3:936–943
7. Dulai JS, Smith EStJ, Rahman T (2020) Acid-sensing ion channel 3: An analgesic target. Channels 15:94–127
8. Sun D, Liu S, Li S, Zhang M, Yang F, Wen M, Shi P, Wang T, Pan M, Chang S, Zhang X, Zhang L, Tian C, Liu L (2020) Structural insights into human acid-sensing ion channel 1a inhibition by snake toxin mambalgin1. eLife *9*: e57096
9. Yooder N, Gouaux E (2020) The His-Gly motif of acid-sensing ion channels resides in a reentrant 'loop' implicated in gating and ion selectivity. ELife 9:e56527
10. Liu Y, Ma J, DesJarlais RL, Hagan R, Rech J, Lin D, Liu C, Miller R, Schoellerman J, Luo J, Letavic M, Grasberger B, Maher M M (2021) Molecular mechanism and structural basis of small-molecule modulation of the gating of acid-sensing ion channel 1. Communications Biology 4:174
11. Paukert M, Chen X, Polleichtner G, Schindelin H, Gründer S (2008) Candidate amino acids involved in H + gating of acid-sensing ion channel 1a. J Biol Chem 283:572–581
12. Tianbo L, Youshan Y, Canessa CM (2009) Interaction of the aromatics Tyr-72/Trp-288 in the interface of the extracellular and transmembrane domains is essential for proton gating of acid-sensing ion channels. J Biol Chem 284:4689–4694
13. Sherwood T, Franke R, Conneely S, Joyner J, PArumugan P, Askwith C (2009) Identification of protein domains that control proton and calcium sensitivity of ASIC1a. J Biol Chem 284:27899–27907
14. Meuzelaar H, Vreede J, Woutersen S (2016) Influence of Glu/Arg, Asp/Arg, and Glu/Lys Salt Bridges on a-Helical Stability and Folding Kinetics. Biophys J 10:2328–2341
15. Sörensen T, Leeb S, Danielsson J, Oliveberg M (2021) Polyanions cause protein destabilization similar to that in live cells. Biochemistry 60:735–746
16. Fiser A, Do RK, Sali A (2000) Modeling of loops in protein structures. Protein Sci 9:1753–1773
17. Anandakrishnan R, Aguilar B, A. V. Onufriev **AV (**2012) **H + + 3.0: Automating pK prediction and the preparation of biomolecular structures for atomistic molecular modeling and simulations**. *Nucleic Acids Res 40*: **W537-W541**
18. *Humphrey W*, *Dalke A*, *Schulten K* (*1996*) *VMD: visual molecular dynamics*. J Mol Graph 14: *33–38*
19. *MacKerell AD et al (1998*) *All-atom empirical potential for molecular modeling and dynamics studies of proteins*. J Phys Chem B 102: *3586–3616*
20. *Phillips JC*, *Braun R*, *Wang W*, *Gumbart J*, *Tajkhorshid E*, *Villa E*, *Chipot C*, *Skeel RD*, *Kalé L*, *Schulten K* (*2005*) *Scalable molecular dynamics with NAMD*. *J Comput Chem 26*: *1781–1802*
21. *Pietra F* (*2020*) Fighting cancer with translation inhibitors: a quantum mechanics view on the complex between the antitumor marine alkaloid agelastatin A and the yeast 80S "ribosome. Structural Chemistry DOI: 10.1007/s11224-020-01706-6

22. *Melo MCR*, *C. Bernardi R*, *Rudack T*, *Scheurer M*, *Riplinger C*, *Phillips JC*, *Maia JDC*, *Rocha GB*, *Ribeiro JV*, *Stone JE*, *Neese F*, *Schulten K*, *Luthey-Schulten Z (2018) NAMD goes quantum: an integrative suite for hybrid simulations*. Nat Methods 15: *351–354*
23. Hybrid QM/MM NAMD, http://www.ks.uiuc.edu/Research/ qmmm/
24. Neese F (2018) Software update: The ORCA program system, version 4.0. Wires Computational Molecular Science 8:e1327
25. Morris GM, Goodsell DS, Halliday RS, Huey R, Hart WE, R. K. Belew RK, Olson AJ (1998) Automated docking using Lamarckian Genetic Algorithm and empirical binding free energy function. *J Computat Chem 19*: 1639–1662
26. *Trott O*, *Olson AJ* (*2010*) *AutoDock Vina*: *improving the speed and accuracy of docking with a new scoring function*, *efficient optimization and multithreading*. *J Comput Chem 31*: *455–461*
27. *GNUPLOT Copyright* (C) 1986–1993, 1998, 2004, 2007 Thomas Williams, Colin Kelley. http://www.gnuplot.info/
28. *Pettersen EF*, *Goddard TD*, *Huang CC*, *Couch GS*, *Greenblatt DM*, *Meng EC*, *Ferrin TE* (*2004*) *UCSF Chimera—a visualization system for exploratory research and analysis*. *J Comput Chem 25*: *1605–1612*
29. *Jmol*: an open-source Java viewer for chemical structures in 3D. http://www.jmol.org/

Figures

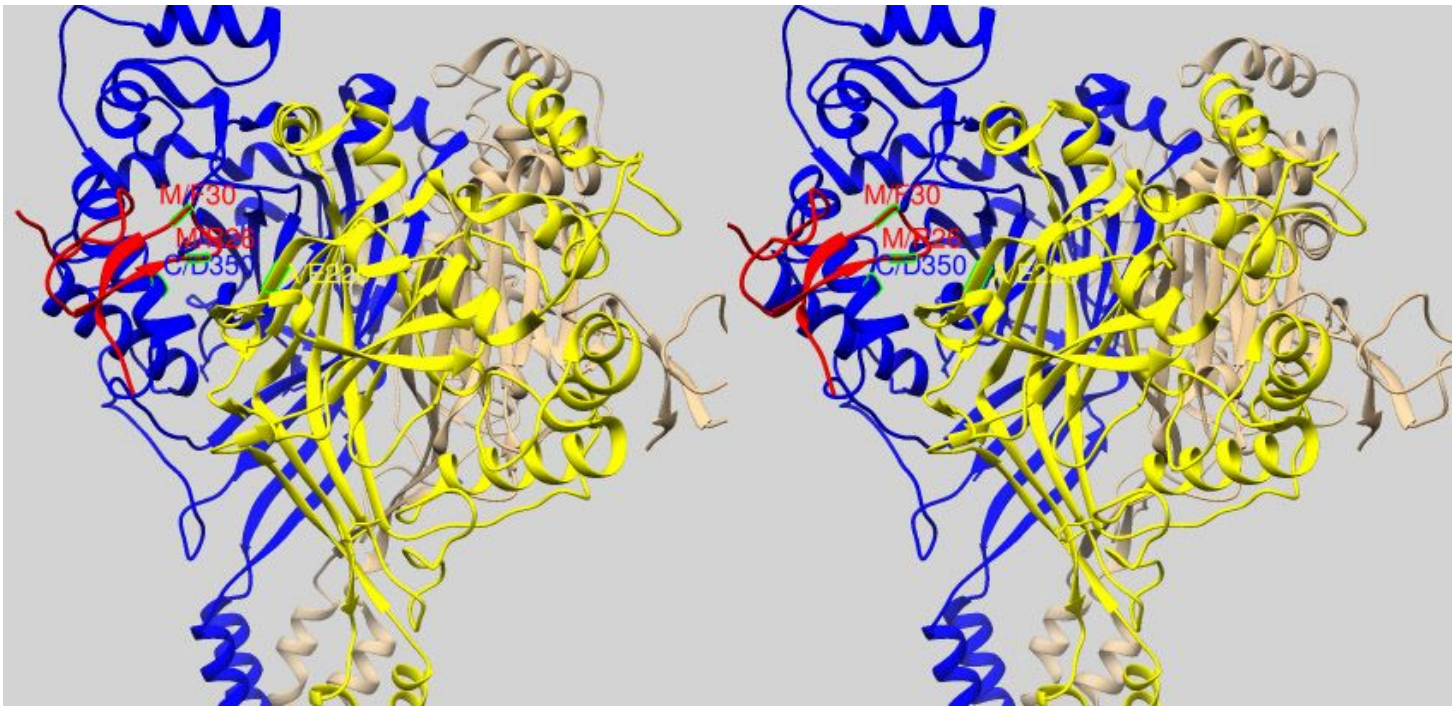

Figure 1

Wall-eye stereo representation based on the crystal structure of the cASIC1a-PcTx1 complex at low pH (5.5) [5]. It is seen that peptide PcTx1 (in red) inserts into the homotrimer receptor between subunit A (in yellow) and C (in blue). Highlighted is residue R26, which interacts with both F30 on the same peptide chain and D350 on chain C of the receptor. Also highlighted on receptor chain A is residue E220, which interacts with R27 (not shown to avoid overlapping of labels) on PcTx1.

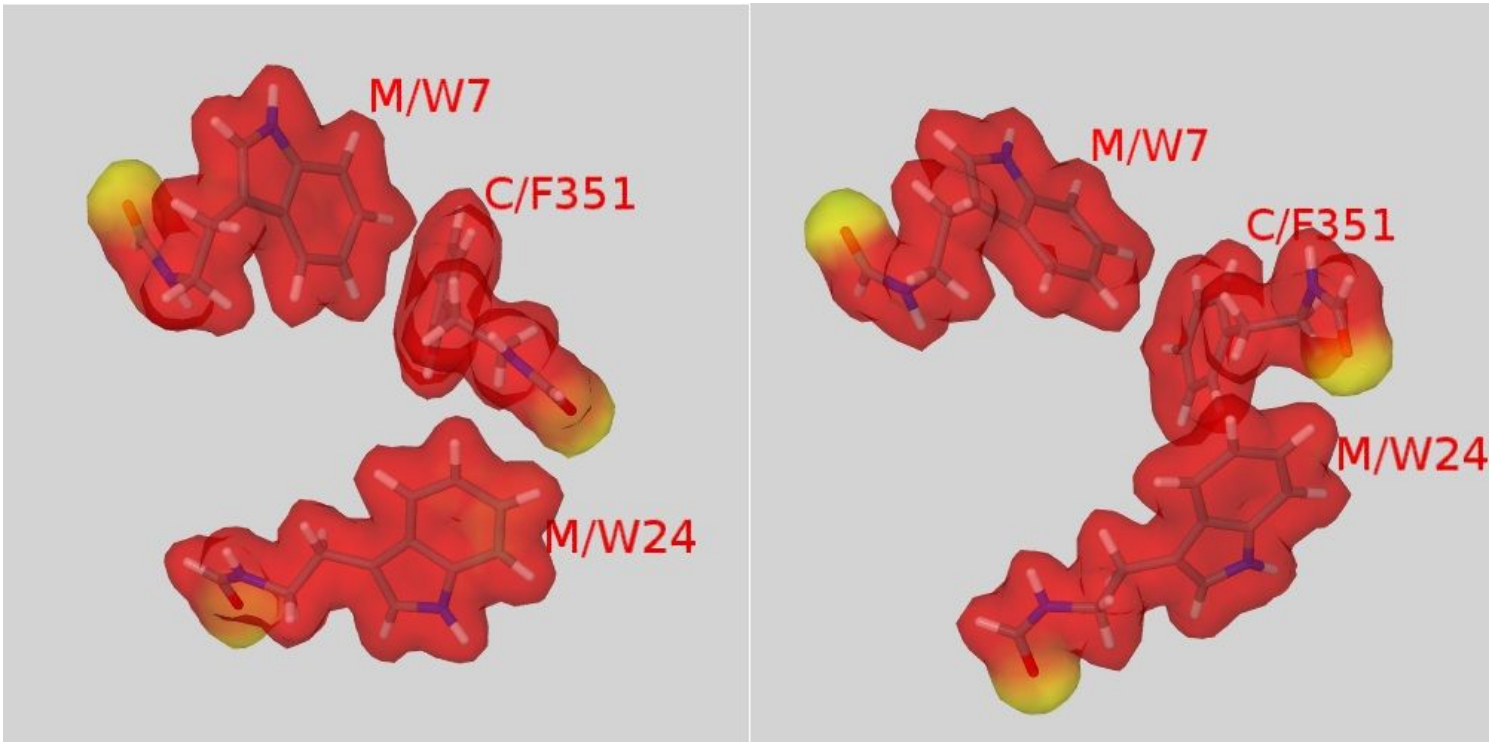

Figure 2

In parallel with data on Table 1, shown here are translucent MEP maps from QM-MM simulations for the group of interactions pivoting on residues W76 and W24 on PcTx1 in complex with cASIC1a at low pH (5.5). Red MEPs stand for high positive potential, degrading toward blue for negative potentials. It is seen that the aromatic 'embrace' formed by residue F351, on cASIC1a subunit C, between W7 and W24 for the low pH (left) and high pH complex (right) do not entail any major electrostatic interaction.

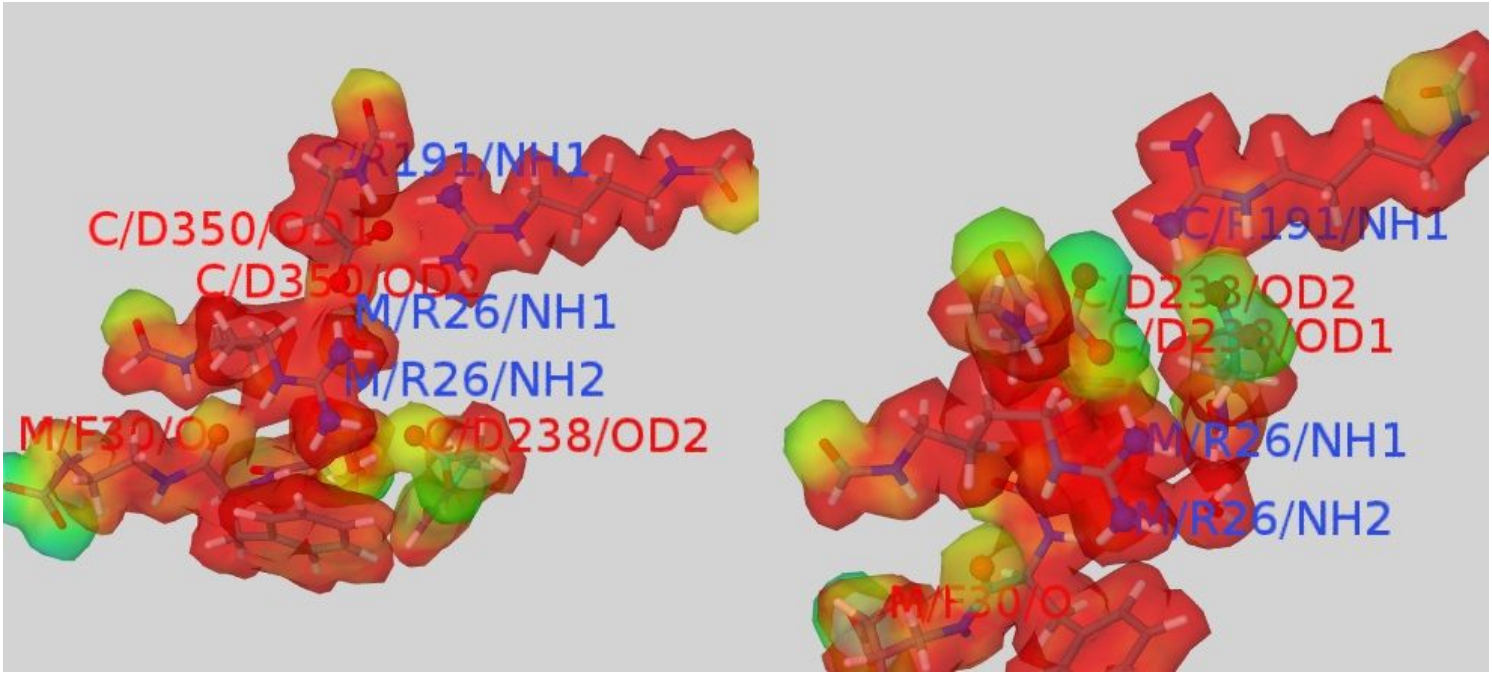

Figure 3

Left: In parallel with data on Table 1, shown here are translucent MEP maps from QM-MM simulations for the group of interactions pivoting on R26 on PcTx1 in complex with cASIC1a at low pH (5.5). Interacting atoms are highlighted at 25% of

the vdW size, in blue for nitrogen and red for oxygen. Red and blue MEPs stand for high positive and high negative potential, respectively, with intermediate colors for intermediate potentials. It is seen that (i) atom NH1 of R26 interacts with atom OD2 of D350 of receptor subunit C, (ii) atom NH2 of R26 interacts with atom OD2 of D238 of receptor subunit C, (iii), internally to the receptor, atom NH1 of R191 interacts with atom OD1 of D350, (iv) internally to the ligand, atom NH2 of R26 interacts with atom O of F30. Right: In parallel with data on Table 2, and for the same above system at high pH (7.25), translucent MEP maps are shown here, showing that the R191/NH1-D350/OD1 interaction at low pH is replaced at high pH by the R191/NH2-D238/OD2 interaction, like in the crystal. Notable involvement of electrostatics in these interactions is indicated by facing opposing colors

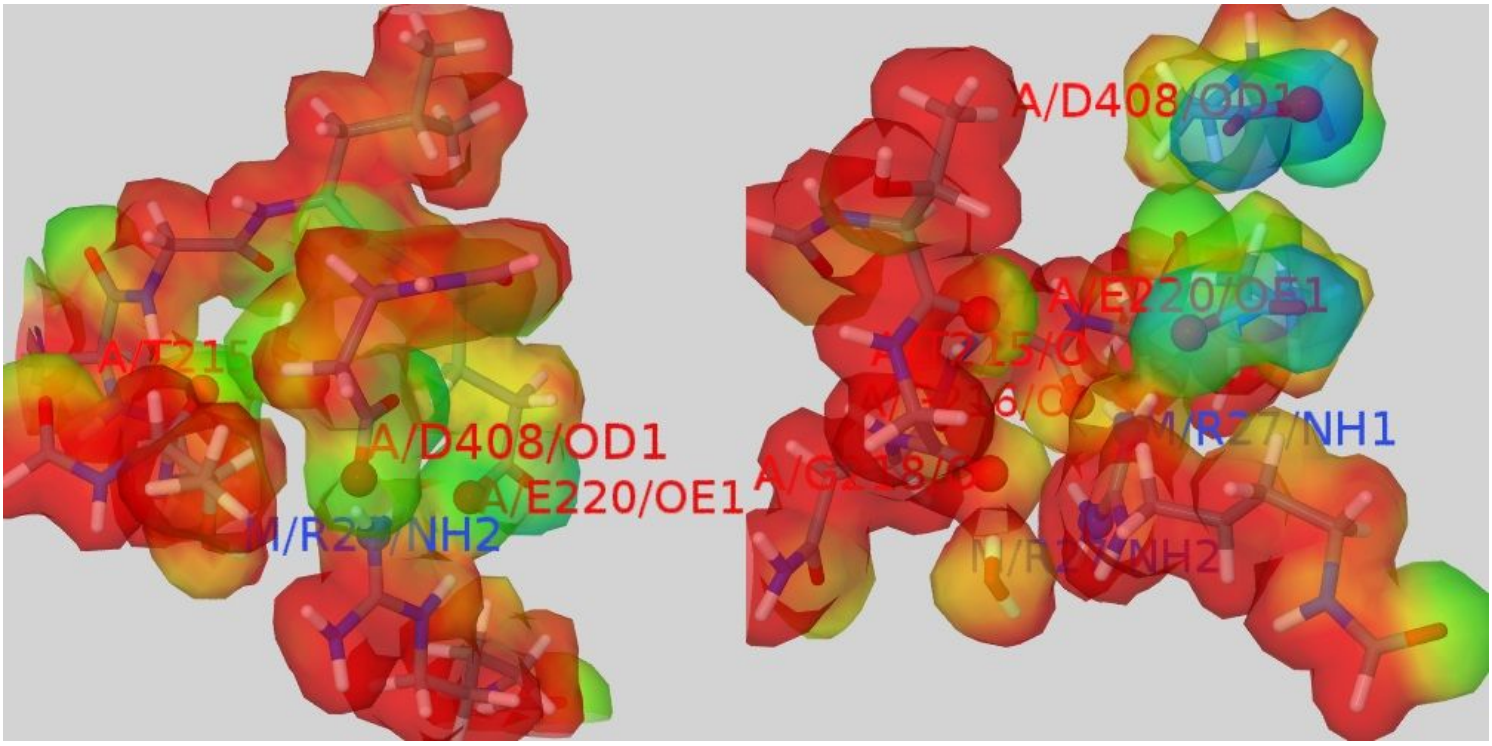

Figure 4

Left: In parallel with data on Table 1 and 2, shown here are translucent MEP maps from QM-MM simulations for the group of interactions pivoting on R27 on PcTx1 in complex with cASIC1a at low pH (5.5). Interacting atoms are highlighted at 25% of the vdW size, in blue for nitrogen and red for oxygen. Red and blue MEPs stand for for high positive and high negative potential, respectively, with intermediate colors for intermediate potentials. It is seen that atom NH2 of R27 interacts with both atom OD1 of D408 and atom OE1 of E220 in the receptor, entailing great electrostatic attraction. Right: In parallel with data on Table 2, and for the same above system at high pH (7.25), it is seen that the receptor conformation has so much changed that the strongly negative end chain of D408 is out of reach by R27.

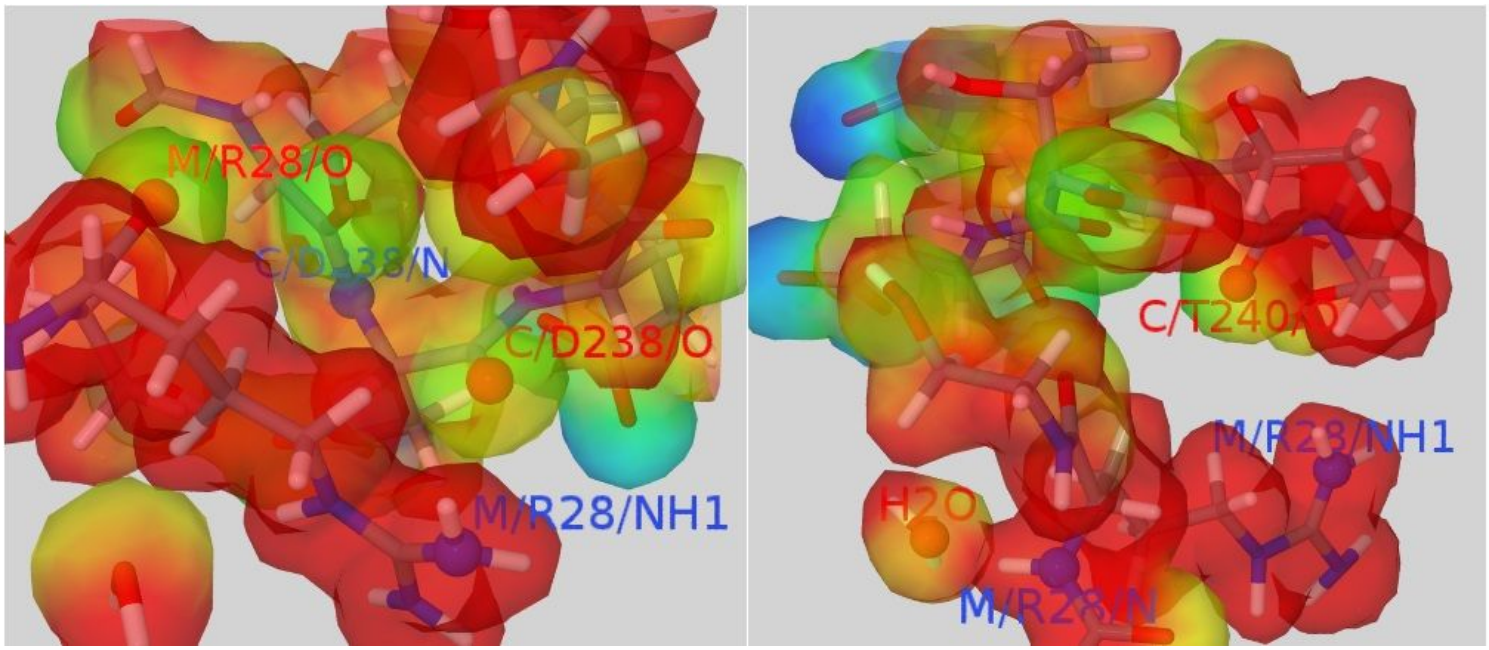

Figure 5

Left: In parallel with data on Table 1, shown here are translucent MEP maps from MD QM-MM simulations for the group of interactions pivoting on R27 on PcTx1 in complex with cASIC1a at low pH (5.5). Interacting atoms are highlighted at 25% of the vdW size, in blue for nitrogen and red for oxygen. Red and blue MEPs stand for highly positive and highly negative potential, respectively, with intermediate colors for intermediate potentials. It is seen that residue R28 of ligand PcTx1 interacts twice with residue D238 of receptor chain: NH1-O and O-N. Right: It is seen, in parallel with Table 2 for the same above system, that at high pH (7.25) the O-N interaction is lost, replaced by interaction with a water molecule. All such interactions entail moderate electrostatics, as indicated by the colors.

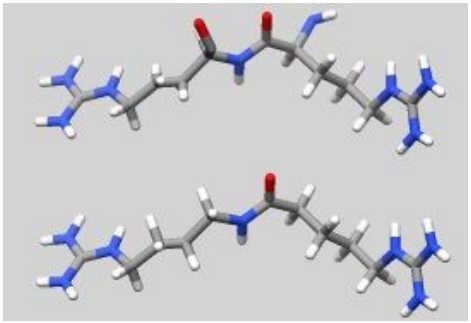

Figure 6

Top: the R26_R27 stretch as excised from PcTx1 of the MD-equilibrated complex with cASIC1a at low pH (5.5). Bottom: The R26_R27 stretch simplified by changing lateral CHO and NH to H for automated docking.

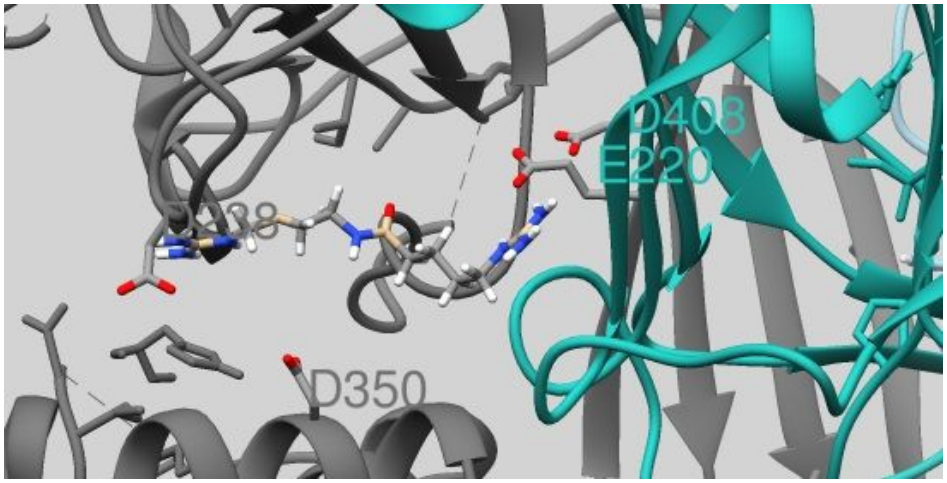

Figure 7

It is seen automated docking on the PcTx1-deprived receptor (cASIC1a) places the modified R26_R27 stretch of Fig. 6 so as to create salt bridges with receptor residues D408 and E220 on chain C and D238 on chain B.